https://doi.org/10.20965/jdr.2021.p0636

Paper:

The Effect of Surface Layer Thickness in a Wide-Area Simulation in Different Models: Susceptibility Mapping of Rainfall-Induced Landslide

Akino Watanabe[*1,†], Akihiko Wakai[*1], Takatsugu Ozaki[*1], Thang Van Nguyen[*1], Takashi Kimura[*2], Go Sato[*3], Kazunori Hayashi[*4], and Nanaha Kitamura[*1]

[*1]Gunma University
1-5-1 Tenjincho, Kiryu, Gunma 376-8515, Japan
[†]Corresponding author, E-mail: t191c051@gunma-u.ac.jp
[*2]Ehime University, Ehime, Japan
[*3]Teikyo Heisei University, Tokyo, Japan
[*4]Okuyama Boring Co., Ltd., Miyagi, Japan
[Received December 1, 2020; accepted March 29, 2021]

In recent years, sediment disaster has frequently been caused by heavy rainfall and has cost many human lives and great property losses. To estimate such risks, Wakai et al. [1] proposed a simplified prediction method to calculate the variation of groundwater levels in natural slopes both at the time of rainfall in wide areas and in real time. To calculate the variation of groundwater levels using this method, the slope conditions (such as material constant and initial conditions) must be determined in advance. This study takes the 2017 heavy rainfall in Northern Kyushu as an example to analyze surface layer thickness, one of the slope conditions that most significantly influences slope stability, over wide areas. The findings reveal that the prediction of slope failure distribution differs depending on how the surface layer thickness and sliding surface are determined.

Keywords: slope failure, groundwater level, seepage flow, numerical simulation, slope stability analysis

1. Introduction

In Japan, the high-performance X-band MP radar is now being deployed nationwide to collect high resolution rainfall data over wide areas. Such observed rainfall data are expected to be applicable to slope disaster management. In order to conduct real time slope stability evaluations over wide areas based on the numerical analysis of these data, it is desirable to adopt a method with a low computation load. Several methods of calculation that can be performed in a short time have been proposed by, for example, Misumi et al. [2], Okimura et al. [3], and Kinoshita et al. [4]. Many previous studies proposed using simplified prediction methods to calculate the variation of groundwater levels based on the Finite Element Method, as presented by Wakai et al. [1] and Ozaki et al. [5]. To acquire accurate solutions using the above-mentioned wide-area analysis, the appropriate material constants and initial conditions should be provided (although this is not easily attainable in wide areas), taking the cost of detailed field surveys and measurements into consideration. Accordingly, to perform such analysis, it is thought that the conditions approximating those on the ground could be determined through estimations based on data from aerial surveys and geological information already available over wide areas. In this study, surface layer thickness, one of the elements that significantly influence the slope stability, is obtained from topographical data; the calculation of the variation of groundwater level and slope stability are then also obtained and the validity examined.

2. Simplified Prediction Method for Calculating Variation in Groundwater Levels

The variation of shallow groundwater levels in natural slopes is calculated, assuming that the slope is characterized by a single geological condition, using two models: vertical infiltration from the ground surface and lateral infiltration of ground water in a saturated zone.

2.1. Modelling Vertical Infiltration Flow

As the model of vertical infiltration used in this study is thoroughly explained by Wakai et al. [1], it is only briefly outlined below. Wakai et al. [1] constructed a simplified prediction model to calculate the rise of groundwater levels with similar accuracy to the FEM in a short period of time based on the analysis of saturated and unsaturated infiltration flows (FEM program: VGFLOW; Cai and Ugai [6]). **Fig. 1** shows an example of the time histories of groundwater levels and the degree of saturation in an unsaturated layer of a slope with semi-infinite length

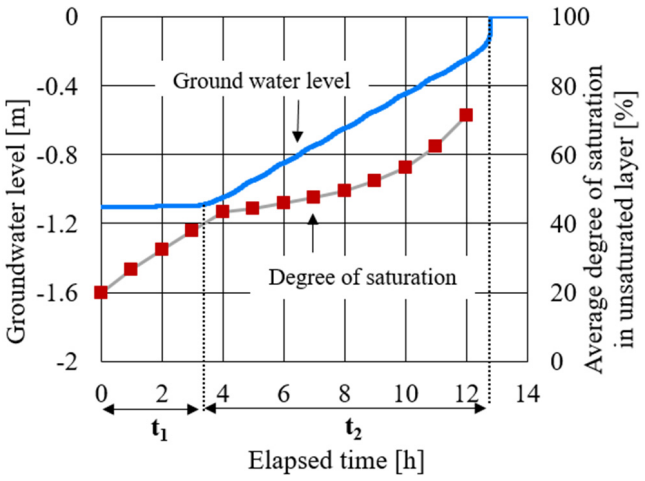

Fig. 1. Time histories of groundwater level and degree of saturation.

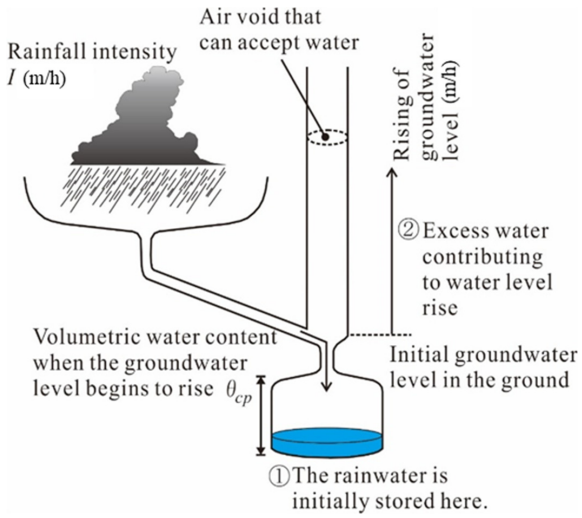

Fig. 2. Concept of the developed model for vertical infiltration in the slope.

under the condition of certain rainfall. These tendencies reveal that groundwater levels hardly rise until the degree of saturation in the unsaturated layer reaches a certain value, even in the case where the start of rainfall and the rising velocity is maintained after groundwater levels begin to rise; Wakai et al.'s [1] model of vertical infiltration takes these time periods into account. The concept of the proposed method is shown in **Fig. 2**. In the case of rainfall with an intensity of I [m/h], where all rainwater infiltrates the ground, with porosity n, depth of the groundwater level before the start of rainfall h [m], and the initial degree of saturation S_{r0} [%], the elapsed time t_1 [h] is expressed by the following equation.

$$t_1 = \frac{h}{I}\left(\theta_{cp} - n\frac{S_{r0}}{100}\right). \quad \ldots\ldots\ldots \quad (1)$$

θ_{cp} indicates the upper limit of the volumetric water content whereby the rainwater infiltrates into unsaturated layers and stays within the ground; in other words, it does not contribute to the rising water level. As the velocity of the saturated zone expanding upwards by filling soil porosity after the water level begins to rise at t_1, velocity v_{wl} will also rise (although this term can be corrected by amplifying α_v). Presuming that the degree of saturation when the groundwater level begins to rise is S_r^*, the elapsed time from when water levels begin to rise until they reach the ground surface t_2 is found by the following equation.

$$t_2 = \frac{h}{v_{wl}} = \frac{n\left(1 - \frac{S_r^*}{100}\right)h}{\alpha_v I}. \quad \ldots\ldots\ldots \quad (2)$$

An event can be estimated in a simplified way by calculating backwards from t_1 and t_2 through a series of analyses to determine the values of the parameters θ_{cp} and α_v under each condition, which can then be applied to the various conditions. From the calculation results of Wakai et al. [1], the parameter θ_{cp} varies depending on the angle of inclination, whereas α_v is constant (= 2.1) regardless of conditions. Additionally, the variation in groundwater levels is caused by vertical infiltration, which is calculated by applying the actual rainfall to Eqs. (1) and (2).

2.2. Modelling the Lateral Infiltration Flow

Surface flow in an unconfined aquifer (i.e., the flow of groundwater along different layers) is governed by the following equation (from the Japanese Association of Groundwater Hydrology) [7].

$$\frac{\partial}{\partial x}\left(T_{xx}\frac{\partial \Phi}{\partial x}\right) + \frac{\partial}{\partial y}\left(T_{yy}\frac{\partial \Phi}{\partial y}\right) = n_e\frac{\partial \Phi}{\partial t}. \quad \ldots \quad (3)$$

In this equation, T_{xx} and T_{yy} indicate the coefficients of transmissibility [m^2/h] found by multiplying the coefficient of permeability K [m/h] with the thickness of an aquifer [m]; N_e represents the effective porosity and Φ [m] is the total head. To find the solution promptly and over a wide area, it is not necessary to carry out a large-scale matrix operation, but the computation load should be low. Therefore, in this method, the approximation is made across time and space according to Kinzelbach's [8] difference calculation algorithm, and the solution is found numerically using the explicit scheme. The wide area behavior of groundwater caused by rainfall is reproduced by calculating the vertical infiltration and the lateral infiltration in the rectangle cells with regular intervals for each time difference.

3. Stability Calculation on the Assumption of a Semi-Infinite Slope

In this study, the slope stability is calculated using the calculated underwater level based on the assumption of a semi-infinite slope, while the slope stability is evaluated at the time of slope failure. The safety factor F_s for slope failure is expressed using the following equation, which

takes the water pressure on a sliding surface into consideration (Yasuda et al. [9]).

$$F_s = \frac{\tau_f}{\tau} = \frac{c' + \left[\gamma_t h_1 + (\gamma_{sat} - \gamma_w) h_2\right] \cos^2\theta \tan\phi'}{(\gamma_t h_1 + \gamma_{sat} h_2) \sin\theta \cos\theta}. \quad (4)$$

In this equation, τ is the driving force that causes sliding, τ_f is the shearing resistance, c' is the adhesive force [kN/m^2], γ_t is the wet unit weight of soil layer [kN/m^3], γ_{sat} is the saturated unit weight of the soil layer [kN/m^3], γ_w is the unit weight of water [kN/m^3], h_1 is the depth from ground surface to groundwater surface [m], h_2 is the depth from groundwater surface to sliding surface [m], θ is the inclination of the slope [°], and ϕ' is the angle of shearing resistance [°].

4. Input Conditions of Analysis

In the heavy rainfall of Northern Kyushu in 2017, a linear precipitation zone that stretched into a belt shape occurred in Fukuoka and Oita Prefectures, triggering record-breaking rainfall in the northern part of Kyushu. In mountainous areas, slope failures were caused everywhere and many of them were classified as surface failure (the Disaster Prevention Research Institute, Kyoto University [10]). By taking this occurrence of heavy rainfall as an example, this study analyses the results and compares the distribution of actual slope failures.

4.1. Common Input Data

The analysis is conducted on an area (**Fig. 3**) that had pelitic schist and granodiorite (in a part of Asakura City, Fukuoka Prefecture), where many slope failures occurred. For the calculation, the DEM measured with 1 m resolution before the occurrence of the disaster was resampled using the DEM measured with 5 m resolution using the method of nearest neighbor interpolation to avoid having too many cells. As many small-scale slope failures with failed slope lengths of 5–10 m were included, the calculation was carried out with 5 m resolution matching that accounted for this scale of slope failure. **Fig. 4** shows the angles of inclination throughout the analysis area. The angle of inclination was calculated and set by the average maximum method using the tool of ArcGIS. Concretely, the value was substituted in each cell, which was calculated by weighing the inverse square of distance using the altitude in the neighborhood of 3×3 adjacent to the cell (ESRI [13], Kamiya et al. [14]). As for the rainfall data, the value observed in the nearest neighbor of each cell was input using the rainfall observed through radar analysis (with a 250 m resolution) by XRAIN on July 5, 2017. As the XRAIN radar analysis was measured each minute, the time interval for the difference calculation was also set to one minute. The distribution of accumulated rainfall in 5 hours is shown in **Fig. 5**. Furthermore, the time history of the rainfall data observed at Point A around the center of the analysis area in **Fig. 5** is shown in **Fig. 6**. For parameters including the coefficient of permeability

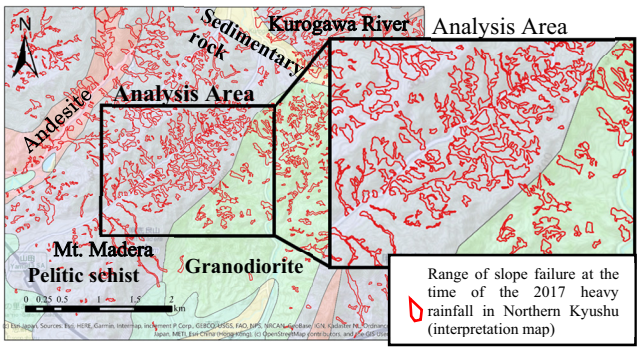

Fig. 3. Analysis area (interpretation map of the damage during July 2017, when the heavy rainfall occurred in Northern Kyushu; this analysis builds on data from the Geospatical Information Authority of Japan [11] and the seamless geological map from the Geological Survey of Japan and the National Institute of Advanced Industrial Science and Technology [12]).

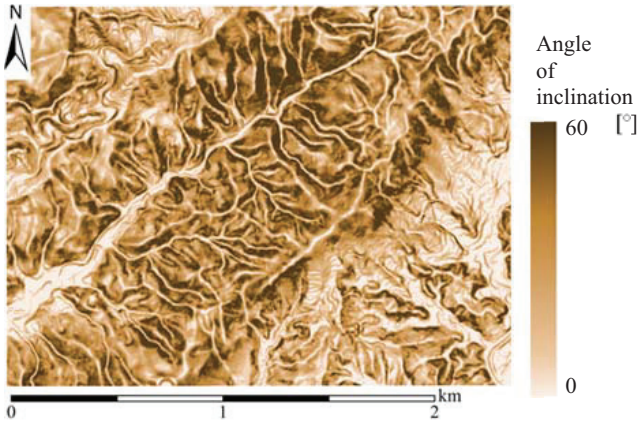

Fig. 4. Angle of inclination in the analyzed area.

to calculate the variation of underwater levels, the representative values for medium sand levels are shown in **Table 1** and provided for the entire analyzed area. The initial degree of saturation was set to 60%. Each physical property value for the stability calculation is shown in **Table 2**. Concerning unit weight and saturated unit weight, the representative values for medium sand levels presented by the Japan Road Association [15] were used. From **Fig. 3**, it can be seen that the analysis area consists of pelitic schist and granodiorite, but mainly pelitic schist. Therefore, the adhesive force measured in the area of pelitic schist by Chiba et al. [16] was set across the entire area of analysis. Furthermore, the value of the angle of shearing resistance was determined with reference to the representative value for medium sand levels in dense conditions, as presented by Yoshimi [17].

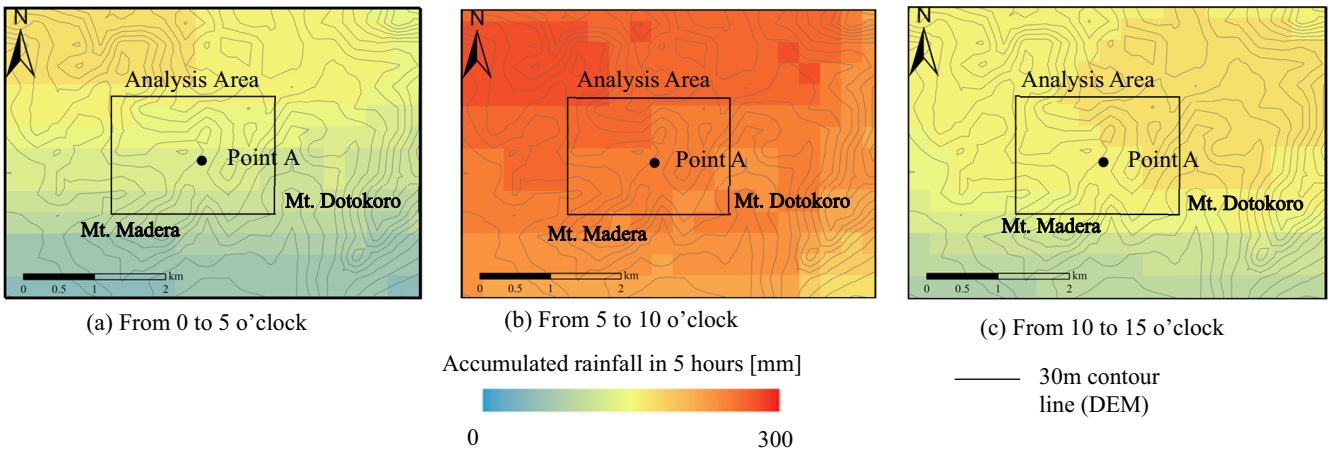

Fig. 5. Development of accumulated rainfall in the analyzed area within 5-hour periods.

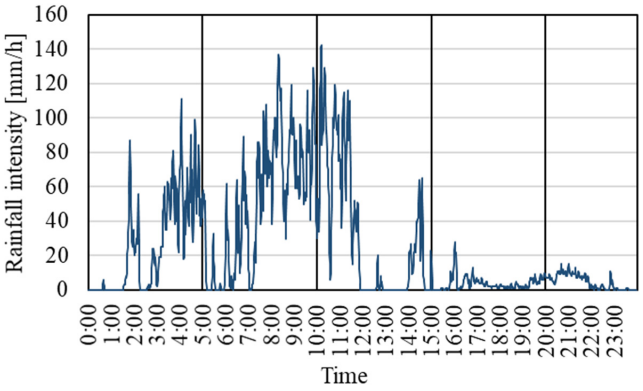

Fig. 6. Rainfall intensity observed in Point A at the time of heavy rainfall in Northern Kyushu on July 5, 2017 (based on XRAIN).

Table 1. Parameters to calculate underground water.

Medium sand levels	
Coefficient of saturated permeability K [m/s]	1.0×10^{-4}
Porosity n	0.3
Initial degree of saturation S_{r0} [%]	60

Table 2. Parameters to calculate the safety factor.

Adhesive force c' [kN/m^2]	9
Wet unit weight of soil layer γ_t [kN/m^3]	18
Saturated unit weight of soil layer γ_{sat} [kN/m^3]	20
Unit weight of water γ_w [kN/m^3]	9.8
Angle of shearing resistance ϕ' [°]	40

4.2. Setting the Surface Layer Thickness

To evaluate the risk of failure, we next examine how to set slope conditions that can significantly influence slope stability. As a result of the sensitivity analysis of each parameter in Eq. (4), Okimura [18] found that the parameter that most significantly influences the safety factor is surface layer thickness. For this reason, the surface layer thickness is set by taking wide-area topography into consideration.

In this study, the surface layer thickness is set using the method proposed by Sakai et al. [19]. Sakai et al. conducted a topographical analysis using data from areal laser measurements to estimate surface layer thickness in an extended wide area. A survey was conducted for the upper stream of Noro River in Yamanashi Prefecture, which is comprised of sedimentary rock (sandstone and mudstone) of the Shimanto group from the Mesozoic era. Multiple regression analysis was performed based on topography indices showing strong correlations with the actual measurements of surface layer thickness using a cone penetration test. The mathematical relation is expressed by the following equation.

$$\begin{aligned} \mathrm{Y} = {} & 0.0321\mathrm{S} + 0.0557\mathrm{U} + 0.0097\mathrm{L} \\ & -7.7727K_1 + 5.0000K_2 - 5.1254 \quad \ldots \quad (5) \end{aligned}$$

In this equation, Y is the estimated surface layer thickness [m], S is the inclination of a slope [°], U is the over ground openness [°], L is the underground openness [°], K_1 is the curvature in the direction of the maximum inclination, and K_2 is the curvature in the direction orthogonal to that of K_1. According to Eq. (5), surface layer thickness depends largely on curvature. The smaller K_1 and the larger K_2, the thicker the surface layer. In other words, the more convex the terrain in the direction of the maximum inclination, and the more concave in the orthogonal direction, the thicker the surface layer. However, because there are negative terms in the equation, surface layer thickness Y could take on a negative value. Therefore, the minimum value of surface layer thickness Y is set at 0.2 m, as in Sakai et al. [19]. Although these results are actually derived from characteristics such as geological features different from the characteristics of the area

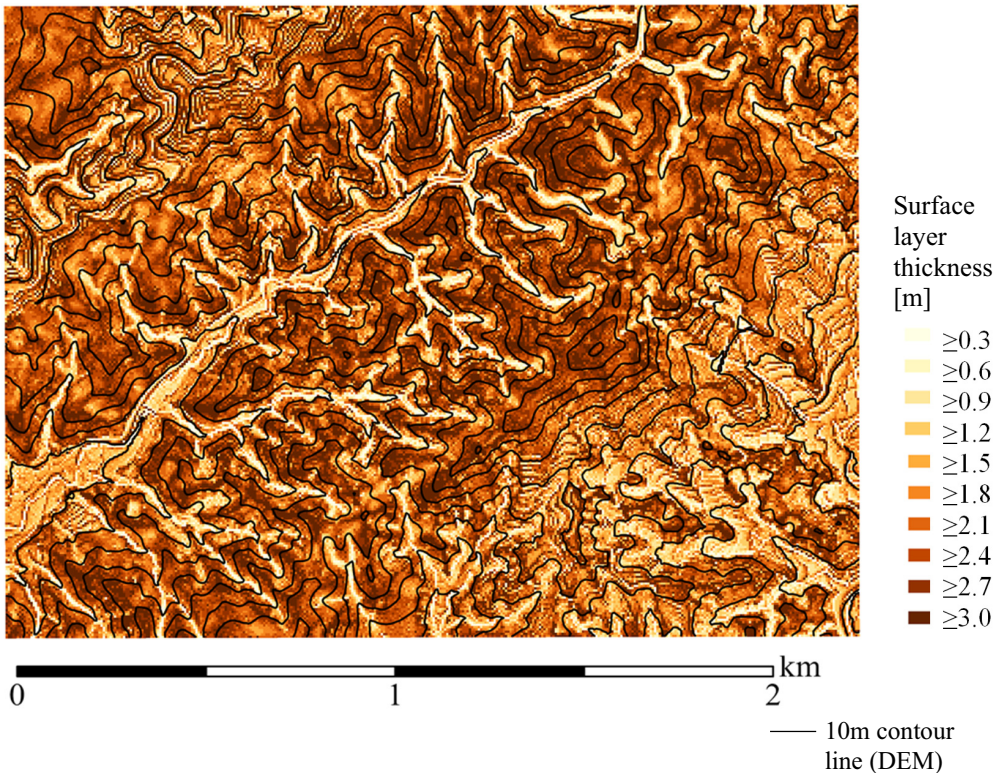

Fig. 7. Results of the estimated surface layer thickness.

covered by this study, and although the results estimated from each topological amount are thought to have different tendencies, the calculation is made using the same equation but on a trial basis. The results of the estimated surface layer thickness are shown in **Fig. 7** and primarily range from 2 to 3 m. The thickness layer along the ridge with smaller K_1 values, which becomes convex in the direction of the maximum inclination, is especially large.

First, referring to the general sliding surface of surface failure indicated by the Japan Society of Erosion Control Engineering [20], the surface layer thickness of 2.0 m is taken across all the cells in the analysis area. Then, the surface layer thickness reflecting the spatial distribution in **Fig. 7** is input for the analysis and the results of two cases are compared. Supposing that the initial groundwater level is located below the surface of the base rock, the thickness value of the initial unsaturated layer (namely, the depth to the base rock) is applied to the initial groundwater level.

5. Analysis Results

5.1. Analysis Results of Groundwater Level

Figure 8 shows the calculation results for groundwater levels in the case where a specific surface layer thickness is set within the analysis area. **Fig. 8** shows that the groundwater level gradually rises when there is intensive rainfall over a long period of time, and reaches close to the ground surface in almost the entire area by around 10 o'clock. It also confirms that slope stability is likely to be lost with heavy rainfall; once the rain calms down, the groundwater level is reduced from the ridges. Next, the calculation results of the variation of underwater levels using surface layer thickness in **Fig. 7** are shown in **Fig. 9**. It is confirmed that groundwater is concentrated at spots where the surface layer thickness is larger than where the surface layer thickness is constant, as shown in **Fig. 8**. It should be noted that there is significant difference between **Figs. 8** and **9** in this regard.

5.2. Analysis Results of Factor of Safety

The stability is calculated using the calculation results of the underwater level described in the previous section, based on the assumption of a semi-infinite slope. The calculation results for the safety factor when surface layer thickness is constant, as well as when the spatial distribution is taken into consideration, are shown in **Fig. 10**. The minimum value of the safety factor during the period of analysis is shown in each cell, and the area regarded as the slope failure site (based on the analysis on the difference in altitude before and after the disaster, which was conducted by the Kyushu Development Bureau, the Minister of Land, Infrastructure, Transport and Tourism [21]), were used for comparison. In the figure, the range of slope failure is shown in a red frame. **Fig. 10** shows that the safety factor falls below 1.0 at many source areas of failure. However, there are some locations where the safety factor does not decrease at the source area of failure and some locations cannot reproduce the site of slope failure.

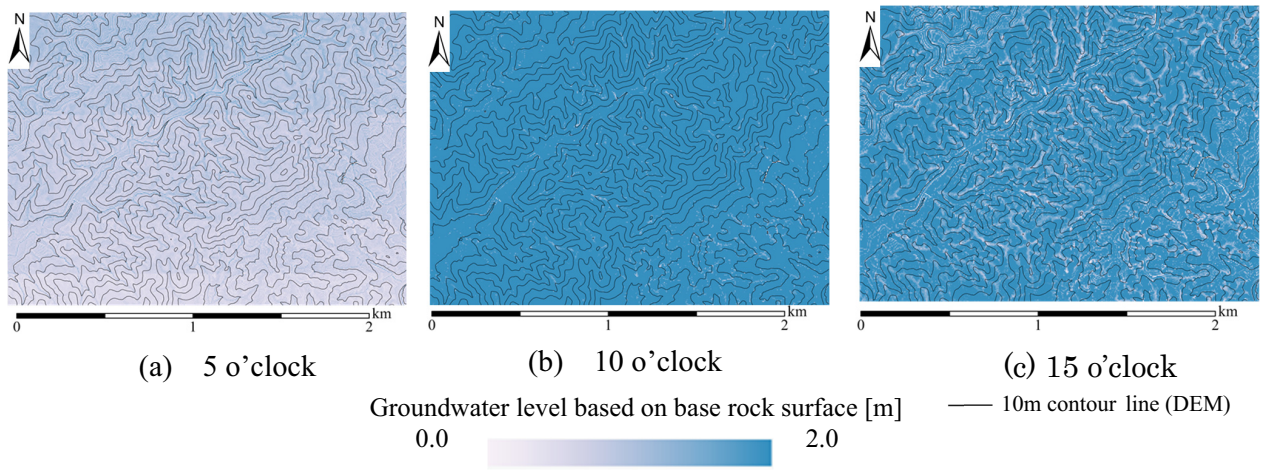

Fig. 8. Distribution of groundwater levels at each time point when the surface layer thickness is constant.

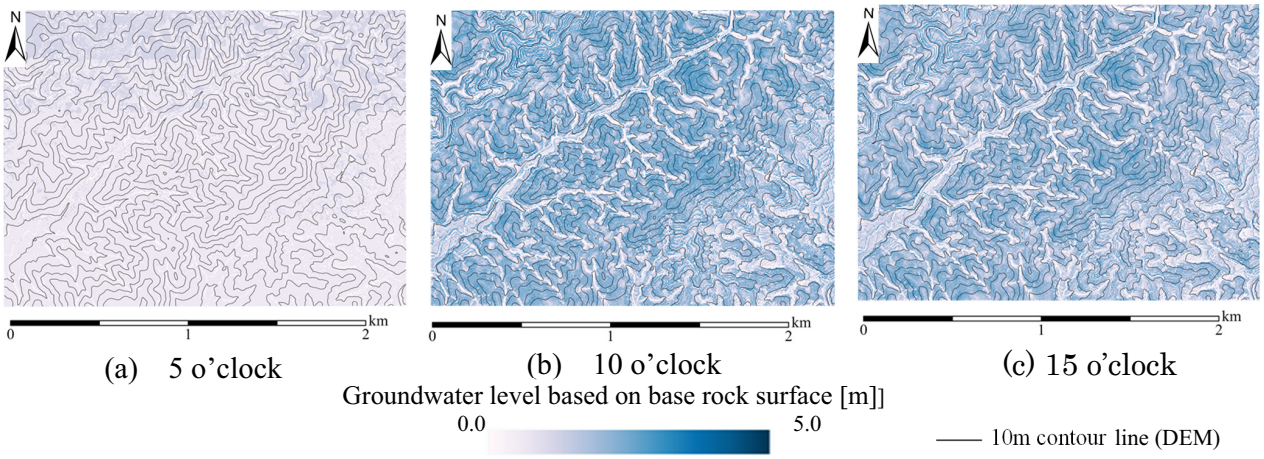

Fig. 9. Distribution of groundwater level at each time point, taking the distribution of surface layer thickness into consideration.

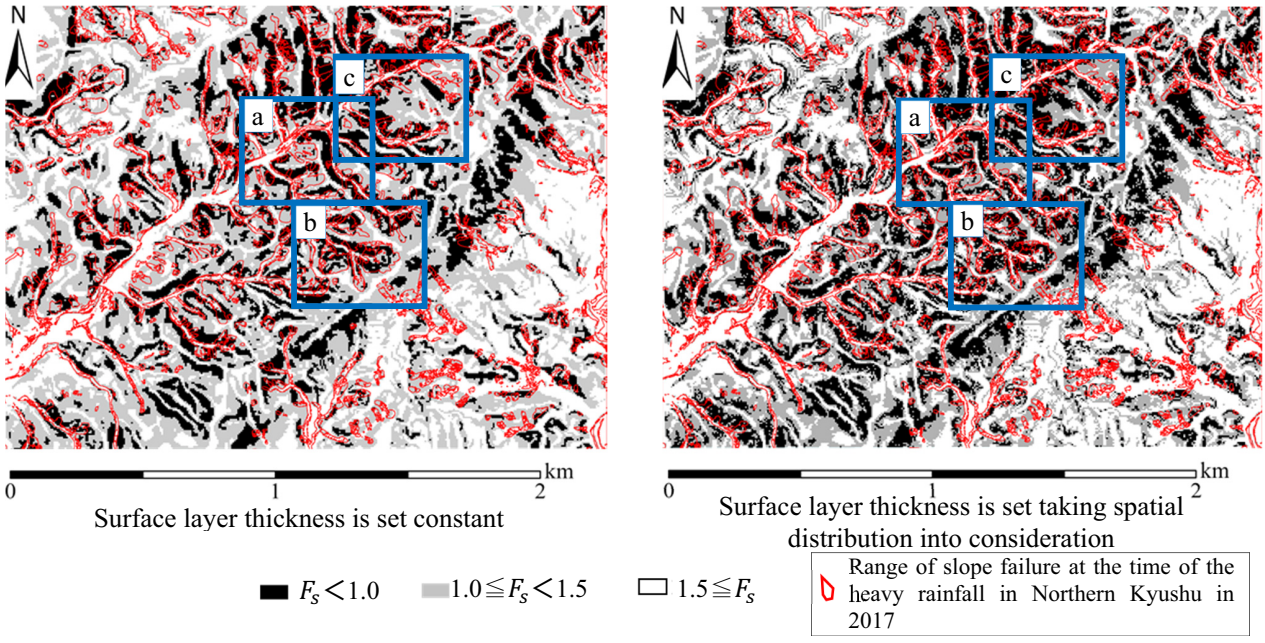

Fig. 10. Results of the minimum safety factor F_s during the analysis period and the distribution of failure.

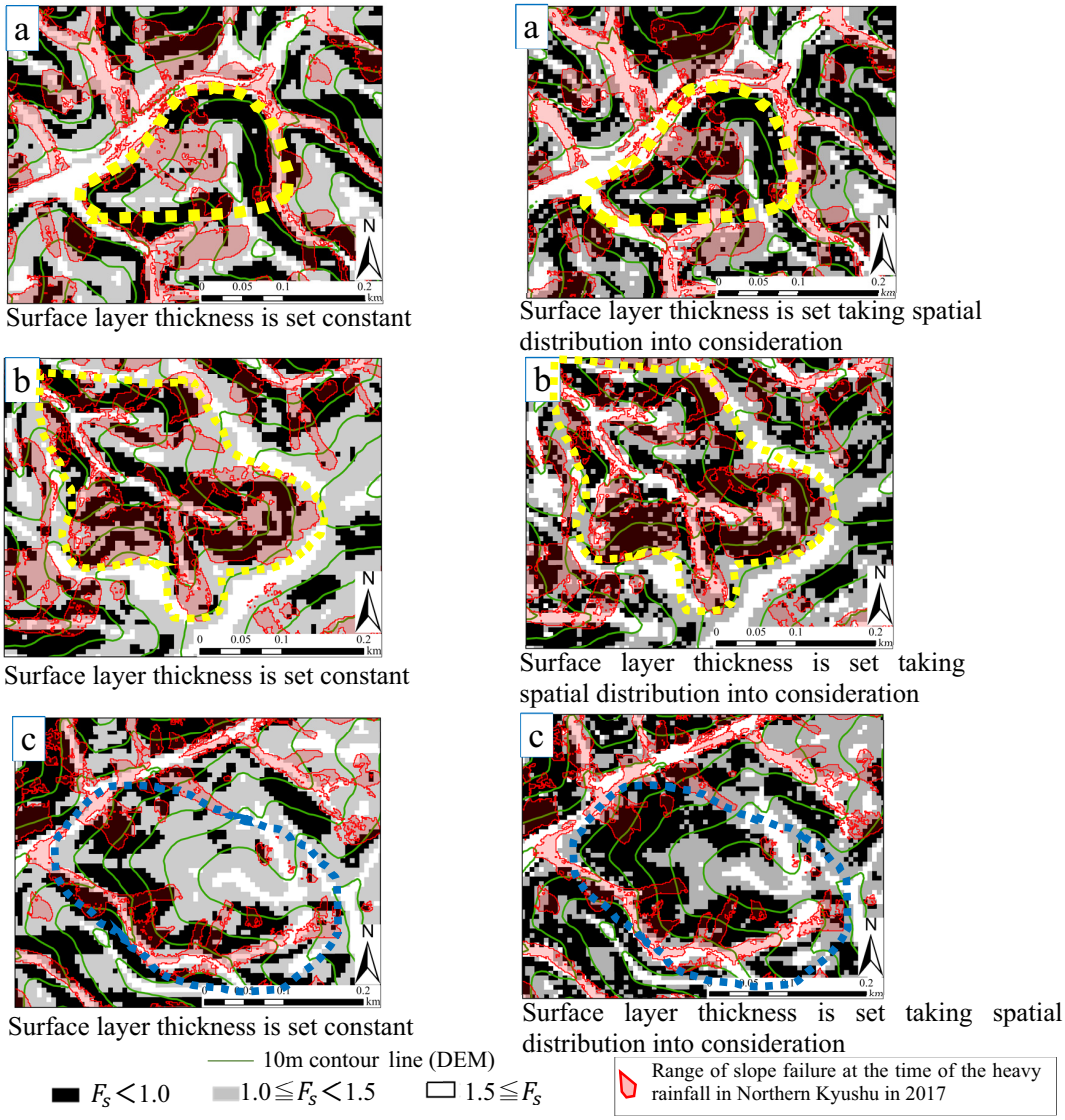

Fig. 11. Calculation results of the minimum safety factor F_s during the analysis period in each area within blue frames in **Fig. 10**, and the distribution of failure.

The comparison results are shown in **Fig. 11** by enlarging the areas marked in blue frames in **Fig. 10**. For example, at the failure sites in the areas indicated with broken yellow lines in **Figs. 11(a)** and **(b)**, the safety factor does not decrease when the surface layer thickness is constant, whereas it falls below 1.0 when the surface layer thickness is set taking the spatial distribution into consideration, matching the actual range of failure better. In the locations where it becomes concave in the direction orthogonal to the maximum inclination, a larger value of the surface layer thickness is calculated by considering the spatial distribution rather than by setting a constant value of 2.0, which is reflected in the figure. In contrast, in the areas indicated by broken blue lines in **Fig. 11(c)**, the results when the surface layer thickness is set at a constant 2.0 m showed a better match with the locations where there were actual slope failures and the safety factor was less than 1.0. When the expanding spatial distribution of surface layer thickness was considered and there was no slope failure, the safety factor was found to be lower. In the locations where it became convex in the direction of the maximum inclination, larger value for the surface layer thickness was found when the spatial distribution of surface layer thickness was considered, rather than when the thickness was set at a constant 2.0 m, which is reflected in the figure.

5.3. Considering the Relationship Between Topological Amounts and Failure Sites

By calculating the safety factor while taking the spatial distribution of surface layer thickness into consideration, the locations matching the distribution of failure with sites that had low safety and other locations that were not matched can be found. In the concave topography between ridges, the risk of overlooking the location of slope failures can be evaluated by increasing the surface layer thickness. In contrast, on a convex ridge in the direc-

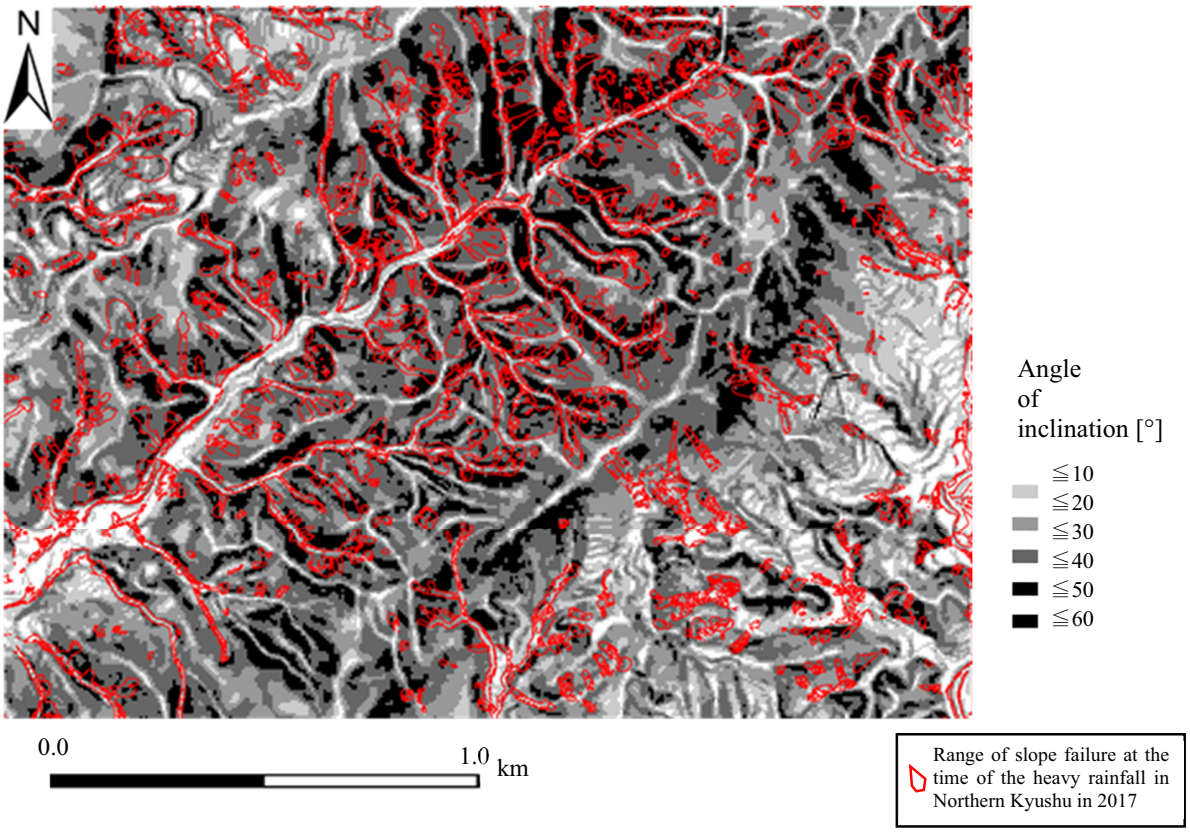

Fig. 12. Distribution of slope failure and the angles of inclination.

tion of the maximum inclination, the number of locations other than the actual failure sites (i.e., where the stability is calculated as being lower) increases when surface layer thickness is enlarged. The equation used in this study to estimate surface layer thickness was derived for sites with different geological features than those found in the analyzed area. Therefore, this equation may express different tendencies from those of the actual slopes in the analysis area. Thus, the precision of the measurements could be improved by considering the equations in light of the topography in question.

Figure 12 shows the distribution of slope failure and the angles of inclination in the analysis area. From **Fig. 12**, it can be concluded that slope failure did not occur in locations with an angle of inclination that exceeded 40°. This tendency is particularly noteworthy in the area of granodiorite that is south of the ridge of the eastern mountain range (**Fig. 3**). It is estimated that rock at a steep location would be naked, and slope failure causing sediment runoff would not occur. However, because the angle of inclination is large, there is a possibility that the safety factor would be lower than the actual figure when performing the stability calculation. To avoid overestimation and judge the risk of a slope more accurately, it seems necessary to extract conditions of the ground itself, including the relation between the angle of inclination and surface layer thickness.

6. Conclusions

In order to evaluate the risk of a landslide disaster over a wide area in real time, this study examined ways to set the wide-area slope conditions, particularly in terms of the conditions of surface layer thickness. The settings of surface layer thickness and the position of sliding surfaces influence the evaluation results of slope stability, and should be performed more accurately by taking the topography into consideration to reproduce the distribution of slope failure. The estimation equation used to set the conditions of surface layer thickness in this study was originally derived for sites with different geological features than the area covered by this study. Thus, the accuracy of the findings could be improved by reflecting the specific characteristics of the analyzed area in future studies. Furthermore, the risk may be overestimated at locations with large inclinations of slope. To avoid such overestimation, it is necessary to more accurately reflect the conditions of a natural slope (e.g., naked rock) in future calculations. Although only the reproduction of spatial distribution of slope failure is examined in this study, the estimation of failure time is also required in practice. In future, the accuracy should be improved in terms of time and space by examining the initial conditions of groundwater and the degree of saturation.

Acknowledgements

Part of this study was supported by JST SICORP "JPMJSC18E3" (Construction of monitoring and the prediction system of landslides). The authors used the rainfall data from XRAIN (the Ministry of Land, Infrastructure, Transport and Tourism), and borrowed the DEM data from the Kyushu Development Bureau (the Ministry of Land, Infrastructure, Transport and Tourism). The authors sincerely appreciate their kindness.

References:

[1] A. Wakai, K. Hori, A. Watanabe, F. Cai, H. Fukazu, S. Goto, and T. Kimura, "A simple prediction model for shallow groundwater level rise in natural slopes based on finite element solutions," J. of the Japan Landslide Society, Vol.56, Special Issue, pp. 227-239, 2019 (in Japanese).

[2] R. Misumi, T. Oguchi, M. Maki, and K. Iwanami, "A real-time forecast of shallow landslides using a distributed rainfall-runoff model," J. of Japan Society for Natural Disaster Science, Vol.23, No.3, pp. 415-432, 2004 (in Japanese).

[3] T. Okimura, N. Torii, Y. Osaki, M. Nambu, and K. Haraguchi, "Construction of real-time type hazard system to predict landslides caused by heavy rainfalls," J. of the Japan Society of Erosion Control Engineering, Vol.63, No.6, pp. 4-12, 2011 (in Japanese).

[4] A. Kinoshita, T. Kanno, A. Okamoto, M. Hitokoto, M. Onodera, M. Sakuraba, and M. Sugiyama, "Construction of real-time hazard map system in Rokko mountain area," J. of the Japan Society of Erosion Control Engineering, Vol.66, No.1, pp. 15-22, 2013 (in Japanese).

[5] T. Ozaki, A. Wakai, A. Watanabe, F. Cai, G. Sato, and T. Kimura, "A simplified model for the infiltration of rainwater in natural slope consisting of fine sands," J. of the Japan Landslide Society, Vol.58, No.2, pp. 57-64, 2021 (in Japanese).

[6] F. Cai and K. Ugai, "Numerical analysis of rainfall effects on slope stability," Int. J. of Geomechanics, Vol.4, No.2, pp. 69-78, 2004.

[7] Japanese Association of Groundwater Hydrology, "Simulation of ground water flow and solute transport," pp. 47-51, Gihodo Shuppan, 2010 (in Japanese).

[8] W. Kinzelbach (Ed.), "Groundwater modelling: An introduction with sample programs in BASIC," pp. 29-35, Elsevier Science Ltd., 1986.

[9] S. Yasuda, Y. Yamada, and T. Katada, "Soil mechanics," pp. 153-154, Ohmsha, Ltd., 2014 (in Japanese).

[10] Disaster Prevention Research Institute, Kyoto University, "Report of the 2017 Northern Kyushu Heavy Rain Disaster Research Mission," p. 49, 2018 (in Japanese).

[11] Geospatial Information Authority of Japan, https://www.gsi.go.jp/BOUSAI/H29hukuoka_ooita-heavyrain.html [accessed July 14, 2019]

[12] Geological Survey of Japan, "Seamless Digital Geological Map of Japan (1:200,000)," https://gbank.gsj.jp/seamless/v2.html [accessed November 22, 2020]

[13] Environmental Systems Research Institute (ESRI), "Raster Surface toolset concepts, How Slope works," https://desktop.arcgis.com/ja/arcmap/10.3/tools/3d-analyst-toolbox/how-slope-works.htm [accessed November 22, 2020]

[14] I. Kamiya, T. Kuroki, and K. Tanaka, "Interpretation of geomorphology and geology using slope gradation map," Geoinformatics, Vol.11, No.1, pp. 11-24, 2000 (in Japanese).

[15] Japan Road Association, "Manual for Asphalt Pavement," p. 114, 1990 (in Japanese).

[16] S. Chiba et al., "Survey case report on a slope that collapsed due to heavy rain in northern Kyushu in 2017 Part 1 – Comparison of characteristics of surface collapsed areas in three geological zones –," JSECE Publication, No.83, pp. 153-154, 2018 (in Japanese).

[17] Y. Yoshimi and Architectural Structure Editorial Committee, "Soil mechanics," p. 97, Shokokusha, 1967 (in Japanese).

[18] T. Okimura, "A method for estimating potential failure depth used for a probable failure predicting model," J. of the Japan Society of Erosion Control Engineering, Vol.42, No.1, pp. 14-21, 1989 (in Japanese).

[19] Y. Sakai, A. Kinoshita, K. Ogawa, and M. Nakata, "Estimation of surface soil layers depth by Terrain Analysis from LiDAR data," J. of the Japan Society of Erosion Control Engineering, Vol.64, No.6, pp. 38-42, 2012 (in Japanese).

[20] The Japan Society of Erosion Control Engineering, "Committee report on basic matters related to landslide," JSECE Publication No.65, p. 12, 2012 (in Japanese).

[21] Kyushu Development Bureau, Ministry of Land, Infrastructure, Transport and Tourism, "Restoration Committee Report on the right bank of the Chikugo River," http://www.qsr.mlit.go.jp/bousai_joho/H29hokubugouu/taisaku.html (in Japanese) [accessed March 18, 2021]

Name:
Akino Watanabe

Affiliation:
CTI Engineering Co., Ltd.

Address:
4-2-20 Harigaya, Urawa-ku, Saitama, Saitama 330-0075, Japan

Name:
Akihiko Wakai

Affiliation:
Professor, Gunma University

Address:
1-5-1 Tenjincho, Kiryu, Gunma 376-8515, Japan

Name:
Takatsugu Ozaki

Affiliation:
Ph.D. Student, Graduate School of Science and Technology, Gunma University

Address:
1-5-1 Tenjincho, Kiryu, Gunma 376-8515, Japan

Name:
Thang Van Nguyen

Affiliation:
Ph.D. Student, Geotechnical Engineering Laboratory, Department of Environmental Engineering Science, Gunma University

Address:
1-5-1 Tenjincho, Kiryu, Gunma 376-8515, Japan

Name:
Takashi Kimura

Affiliation:
Assistant Professor, Graduate School of Agriculture, Ehime University
Address:
3-5-7 Tarumi, Matsuyama, Ehime 790-8566, Japan

Name:
Go Sato

Affiliation:
Professor, Graduate School of Environmental Informations, Teikyo Heisei University
Address:
4-21-2 Nakano, Tokyo 164-8530, Japan

Name:
Kazunori Hayashi

Affiliation:
Assistant Manager, Okuyama Boring Co., Ltd.
Address:
13-18-306 Futsukamachi, Aoba-ku, Sendai, Miyagi 980-0802, Japan

Name:
Nanaha Kitamura

Affiliation:
Undergraduate Student, Geotechnical Engineering Laboratory, Department of Environmental Engineering Science, Gunma University
Address:
1-5-1 Tenjincho, Kiryu, Gunma 376-8515, Japan